Feb 1983

P-726

A PROPOSAL TO STUDY HIGH ENERGY $\bar{p}p$ INTERACTIONS AT THE FERMILAB COLLIDER WITH A 4_π HIGH RESOLUTION ELECTROMAGNETIC/HADRONIC CALORIMETER

M. Abolins, R. Brock, W. Bieterle, L. Cormell, B. Cox, J. Lebritton, K. Lai, D. Owen, W. Selove, G. Theodosiou, F. Turkot

Univ. of Arizona - Fermilab - Michigan State Univ. - Univ. of Pennsylvania

Abstract

We propose to build a 4_π non-magnetic electromagnetic/hadronic detector with good hadronic resolution and the highest electromagnetic resolution that is currently feasible in order to study the decays of heavy particles such as Z^o, and heavy quarkonium states into electromagnetic products ($e^\pm, \gamma$). This detector will also be able to perform missing p_T measurements to detect the existence of such phenomena as new neutrino flavors and gluinos and to study such 'standard' phenomena as W decay to $e^\pm\nu$.

Correspondents:

M. Abolins - Michigan State Univ. (517/353-1677)
B. Cox - Fermilab (312/840-3152)
W. Selove - Univ. of Pennsylvania (215/898-8159)

Contents

I. Physics Objectives and Capabilities

Many exciting phenomena are expected to occur in $\bar{p}p$ collisions at high energies at the Fermilab collider ($\sqrt{s} \sim 2000$ GeV). Many of these new phenomena are manifested by the production of electrons, photons, and neutrinos in the interactions.[1] With the higher energy and the luminosity which is anticipated for the DØ collision region, the detailed study of the production of the neutral intermediate boson, Z^0,[2] and its subsequent decay into e^+e^- becomes possible. In addition the detection and study of heavy quarkonium states which decay into $e^{\pm}$ and photons should be a prime objective.[3,4] The study of $W^{\pm}$ production and decay to $e^{\pm}\nu$ at the higher energy of the Fermilab Collider should become a 'routine' measurement. But the most exciting prospect in exploring this new energy regime is the possibility of finding something unexpected. While there is no unique prescription of how to do this, recent history along with current theoretical speculations[5,6,7] suggest that the construction of a detector with optimal electromagnetic resolution coupled with the capability of measuring missing p_T is a sensible strategy.

Therefore, we propose to build a non-magnetic 4π electromagnetic and hadronic detector for the DØ experimental area which will have unique capabilities for studying known or expected phenomena and for detecting the completely unexpected. This detector will have the best possible electromagnetic resolution by virtue of several unique features, and will have excellent capability for analyzing hadronic events of particularly interesting types. For electrons and photons the detector will have outstanding resolution and unusually fine gain stability, together with high immunity

against radiation damage because of the use of scintillating glass, vacuum photodiodes for readout, and fine tower segmentation to handle high multiplicity events without deterioration of resolution. With this unique scintillation glass e-m calorimeter, together with the gas sampling hadron calorimeter, this detector will have a capability equal to or better than any proposed or existing collider detector to study:

1) Z^0 decay into e^+e^- with a precision measurement of the Z^0 width. The scintillation glass electromagnetic calorimeter will provide the best possible resolution and control of the systematics of this measurement.

2) Quarkonium decay into e^+e^- or $e^+e^-\gamma$. The superior energy resolution of the scintillation glass calorimeter will be necessary to achieve clean separation of any level structure which may be present in decays of heavy quark-antiquark states into e^+e^- or $e^+e^-\gamma$.

3) The detection and measurement of events with missing p_T with good resolution. This technique has already proved its value in the discovery and measurement of the W boson by UA1 and UA2.[8] With nearly complete coverage of the solid angle we will be sensitive to the production of Z^0's with substantial p_T which decay into $\nu\bar{\nu}$ and to the production of new families of particles with undetected decay products which give rise to missing p_T. A particular example of such a decay would be that of a gluino into $q\bar{q}$ photino as suggested by supersymmetry schemes.[5]

Besides the unique opportunities made possible by the electromagnetic detector and the 4π hadronic calorimeter coverage, our apparatus is well suited because of its fine tower segmentation and resolution to the analysis of more copiously produced phenomena such as high p_T quark or gluon jets, high mass states decaying hadronically, Drell Yan processes and many others. The detection, measurement and analysis of these phenomena by our detector because of the different techniques used (high resolution calorimetry, no magnetic field, etc.) will be complementary for the most part to measurements made by other detectors with magnetic analysis such as CDF, UA1 and UA2 and should prove to be invaluable.

II. Experimental Area Considerations

The detector system shown in Fig. 1 can be contained in a rectangular volume that is 12 m along the beam direction and 3 m by 3 m in transverse dimensions. To accommodate the detector the present elevation of the tunnel floor needs to be lowered; for the central ±3 m of the detector a 3.5 m lowering is required, for the 3 m end sections a 2 m lowering will suffice. It is envisioned that the entire detector system would be mounted on rails and move into position from outside the ring. Crane coverage of 20 tons will be adequate.

In order to allow antiproton accumulation during data taking and minimize radiation damage effects to the e-m calorimeter, it is necessary that the Main Ring beam passes around the detector; this implies an overpass similar to that at BØ. The difference being that the Main Ring beam need only be raised 2.5 m compared to the 5 m at BØ.

With regard to the low-beta insertion, we require a β^* of 2 m ($\sim$ circular beam) and a free space of ±6 m about the interaction region along the beam direction. We anticipate a bunch length[9] with $\sigma \sim 40$ cm for the purposes of the calculations contained in this proposal.

III. Detector

A) General Considerations

The detector design parameters are chosen to optimize the measurement of electrons and photons with the best practical resolution and stability and the lowest possible systematics, and to detect and measure missing p_T with good resolution. In addition the searches and measurements which are proposed require good luminosity and good sensitivity. All of these objectives have to be accomplished at a reasonable cost. These salient considerations lead us to the following general choices for our detector:

1) Nearly 4π coverage for tracking and electromagnetic and hadronic calorimetry to maximize rates and minimize loss of p_T down the beam in a given event.

2) A detector compact both longitudinally ($< \pm$ 6 m) and transversely along the beam directions. This compactness will allow insertion of low beta quadrupoles for maximum luminosity and will minimize costs.

3) Matching tower structure for both the electromagnetic and hadronic calorimetry with fine segmentation in pseudorapidity (η) and ϕ ($\Delta\eta \curvearrowvee 0.21$ and $\Delta\phi \curvearrowvee 12^{\circ}$ for the entire 4π of coverage). One central concern in the detector design has been to insure that these electromagnetic particles can be clearly separated from the high multiplicity of charged and neutral hadrons in $\sqrt{s}$ = 2000 $\bar{p}p$ final states ($\langle N_h \rangle \curvearrowvee 50$; $\langle dN_h/dy \rangle \curvearrowvee 6$, but not infrequently 10 or more, as estimated from the UA1 results).[10] Therefore we have sought to minimize the shower sharing between optically isolated units and to

minimize actual hadron-photon-electron overlaps, effects which confuse and degrade the mass resolution of any final states.

The most serious of these two types of overlap confusions is that where an interesting signal in a particular electromagnetic calorimeter segment is subject to contamination by the tail of a shower from a distant particle. In particular, hadronic showers have extensive transverse spreads. Measurements in the E-609 calorimeter indicate that 20 to 50 GeV hadrons frequently deposit as much as 1 GeV of energy 30 to 40 cm from the impact point. A strip design is much more vulnerable to contamination at the 1% level than is a tower design having a comparable 'small' dimension. This contamination may lead to unknowable systematic uncertainties in shower energy reconstruction and will be minimized in a tower design.

A less serious but still troublesome type of overlap is that which arises from direct hadron-photon-electron overlaps in a particular tower. This corresponds in most cases to the loss of an interesting event rather than a nasty correction to the reconstructed energy of an electron or photon. We estimate from the multiplicity measured at the CERN collider approximately scaled to Fermilab collider energies that a tower configuration of our design will have less than 1% loss of events due to direct overlaps while a strip design might experience a loss of order 10% or greater.

4) Scintillation glass (see Appendix A) as the material of the electromagnetic detector rather than lead glass.

a) Superior energy resolution. The photon statistics contribution to the energy resolution has been measured to be $\sigma/E \backsim 1.1\%/\sqrt{E}$ by E-705[11] vs. $\sigma/E \backsim 4.3\%/\sqrt{E}$ measured for lead glass.[12,13]

b) Superior resistance to radiation damage. Long-term stability of the electromagnetic detector will be a central problem because of the difficulties of calibrating each counter to the accuracy desired in place in the DØ experimental area. SCG1-C scintillation glass has been measured by the Fermilab - McGill - Athens collaboration (E-705)[14] and the experimenters of Ref. 15 to be much more resistant to radiation darkening than lead glass. The E-705 measurements are summarized in Appendix A and Fig. 8. At a wavelength of 436 nm a 10^{10} GeV/cm^2 dose causes a 3% loss of transmission through the SCG1-C Ohara scintillation glass as measured in the direction of the beam. The same dose causes a 60% loss of transmission in SF5 lead glass at the same wavelength. The deposition of energy in a 10^7 seconds experiment with luminosity of 5×10^{29} cm^{-2}/sec will be approximately 10^9 to 10^{10} GeV/cm^2 (depending on the region of the detector) for 'ideally' clean operation of the machine. In the case of much larger doses ($\geq 10^{12}$ GeV/cm^2) the damage level in the scintillating glass, as indicated in Fig. 8, 'saturates' with losses which vary from 5% at longer wavelengths to 60-70% at 436 nm. The SF5 lead glass continues to suffer damage and becomes completely black at 10^{12} GeV/cm^2.

c) The increased light output of the scintillation glass relative to that of lead glass. This factor has been measured[11] to be 5.1 ± 0.3 by the E-705 collaboration. A large fraction of this is scintillation light produced by the Ce_2O_3 of the glass. This allows the glass calorimeter to give a good measurement of the amount of energy deposited by a hadronic shower and together with the hadron calorimeter placed behind it to provide very good energy resolution for single hadrons and jets. The increased light output makes feasible the use of vacuum photodiodes[16,17] (see Appendix B) allowing this detector to have a tower structure, to be compact, and to have much enhanced gain stability over any strip design utilizing photomultipliers. The use of a set of only three photodiodes for reconstruction of the major part of a given shower in our scintillation glass electromagnetic detector (rather than the more than 10 photomultipliers needed to measure a shower in a lead glass strip design) will give excellent resolution and stability. The importance of gain stability is enhanced at higher energies, in particular for $e^{\pm}$ coming from Z^0 decays, where systematics dominate the energy resolution.

5. Gas sampling for the hadron calorimetry. Impressive advances[18] have been made in the last two years in the energy resolution of gas sampling calorimetry operating in the saturated avalanche mode. In addition the use of conductive plastic tubes and pads for readout makes possible fine granularity at a relatively low cost. These

features along with the immunity of the system to even extremely high radiation doses makes gas sampling an obvious and very attractive choice for the hadron calorimetry.

B) Detector Design

The considerations enumerated above lead to the detector design shown in Fig. 1. The detector consists of the following main components: tracking chambers TC1-TC4, the electromagnetic scintillation glass calorimeter which has central (CEM) and forward (FEM) parts and a hadron calorimeter which has central (CH), forward (FH), and very forward (VFEM/VFH) parts. These components are described below.

1) Tracking Chambers

The tracking chamber locations (TC1,2,3,4) are indicated in Fig. 1b. The chambers in the central region (TC1) are a combination of cylindrical proportional and drift chambers which detect tracks with scattering angles in the range $20^{\circ} < \theta < 160^{\circ}$ where θ is the polar angle with respect to the antiproton direction. The forward regions (TC2 - TC4) contain planar proportional chambers which cover the scattering angular ranges $0.7^{\circ} < \theta < 30^{\circ}$ and $150^{\circ} < \theta < 179.3^{\circ}$. In all regions there is 2π coverage of ϕ, the azimuthal angle.

The chambers in the forward regions are planar proportional chambers. The planes are oriented perpendicular to the beam direction (Z axis) and have a central hole to accommodate the beam pipe. The chamber positions range from 57 cm to 480 cm from the center of the intersection region.

The chambers are arranged in groups of four planes per module with wire orientations of $\phi = 0^{\circ}$, 45°, 90°, and 135°. In order to assist the pattern recognition of the high density track region near the beam axis the last plane of each region is equipped with cathode readout pads. These pads are of order 1 cm^2 in size and are arranged to form a 20 cm radius disk centered on the beam axis.

The total number of readout channels for the planar chambers is 38K wires and 7.5K cathode pads. Additional chamber parameters are listed in Table I.

The central region contains four cylindrical proportional wire chambers (CPWC) and one cylindrical drift chamber arranged as shown in Fig. 2. The chambers vary in radius from 12 cm to 30 cm. The inner three chambers (2 CPWC's and the drift chamber) are 110 cm in length while the outer two CPWCs are 90 cm long. The CPWCs have anode and cathode strip readout and measure one space point per plane per track. The drift chamber also determines space points via drift time and charge division measurements. The CPWCs have a total of 2640 sense wires and 2680 cathode readout channels. The drift chamber has 480 sense wires. The cylindrical chamber parameters are given in Table II.

The design of the cylindrical CPWCs is similar to that of the CLEO beam pipe chambers[19] and to that of the UA2 CPWC vertex chambers[20]. A sketch of a CPWC appears in Fig. 3. The cylindrical cathode configuration is constructed from a sandwich of 0.01" mylar and resin foam. The chambers are oriented with their wires parallel

to the beam and with the cylinder axis coinciding with the beam axis. Both cathodes of each gap are equipped with readout strips. The readout strips of the inner cathode are a set of rings oriented at 90° to the Z axis. The outer cathode readout configuration is a set of parallel helical strips oriented at 45° to the Z axis. The helical strips are broken into several independent sections, each with its own readout in order to reduce the frequency of multiple hits. For the inner two CPWCs, there are four sections with the breaks at $Z = \pm 35$ and 0 cm. The outer two CPWCs have two sections each, separated at $Z = 0$. The pulse height of all hits on both the sense wires and cathode strips is recorded and is used to help with strip/sense wire hit correlations as well as to determine the centroid of the cathode signal of each track.

The cylindrical drift chamber is similar to the design used in the JADE detector[21]. As in the CPWCs, the chamber is a cylinder with its wires parallel to the beam and its axis coinciding with the beam axis. The chamber is divided into 60 cells, each covering 6° in ϕ. Each cell contains 8 sense wires which are instrumented for drift and charge division measurements.

2) Electromagnetic Calorimeter

The electromagnetic detector consists of three shells of scintillation glass of thicknesses 4, 6 and 10 radiation lengths. There is a three shell central region (CEM) extending from $\theta \sim 30^{\circ}$ to $\theta = 150^{\circ}$. Each of the two forward electromagnetic detectors (FEM)

covers the angular range from 4.8° to 30° and has the same shell structure as the central region. The inner radii of the shells in the central region of the detector are 60 cm, 81.4 cm and 111.5 cm. The FEM shells have inner radii of 155, 176.4 and 206.5 cm respectively. Both the forward and the central electromagnetic detector have a finely segmented tower structure with the segmentation chosen to be $\Delta\eta = 0.21$ and $\Delta\phi = 12^{\circ}$. The 4 cm space between each shell contains the vacuum photodiodes (see Appendix B) which detect the light from the elements of the scintillation glass shells. There are 840 towers with 2520 elements in the three shells of the electromagnetic detector. There are 14 rings (as measured by $\Delta\theta$ intervals from the beam direction) for each of the shells from 4.8 to 90° and 30 $\Delta\phi$ intervals from 0 to 2π. The total weight of the scintillation glass detector is approximately 54 tons. The parameters of the e-m calorimeters are summarized in Table III.

Studies of the contributions to the electromagnetic resolution possible with scintillation glass have been performed, some of which have already been referred to in Sect. III.A of this proposal. The photon statistics contribution ($\sigma/E \backsim 1.13 \pm 0.33\%/\sqrt{E}$) is minimal above 20 GeV. The stability of the device because of the use of photodiodes against gain drift and because of the relative immunity against radiation damage due to the use of scintillation glass lead us to estimate that energy independent systematic uncertainties can be maintained at the 0.7% level. The tower structure will minimize degradation of the reconstruction of electron or photon energies.

The position measurements of electron or photon induced showers are achieved by gas sampling pad chambers which are positioned in the space between the first and second shells of the CEM and FEM. (See Fig. 2.) Each such chamber has the shape of the outer surface of an orange slice with the anode wires stretched perpendicular to the direction of the bend of the surface. There are 30 chambers in the CEM and a similar number in the forward electromagnetic detectors. The pad size has been chosen to be approximately 9 cm^2. This segmentation has been estimated from measurements[22] made by E-705 to lead to a position resolution of $< 1.5\ cm/\sqrt{E(GeV)}$. The CEM and the two FEM regions have 6K pads each.

Finally the three shells of the detector provide three samplings of the longitudinal shower profile at 4,10, and 20 radiation lengths in order to reject hadron contamination of electromagnetic signals. In addition the electromagnetic calorimeter is backed up by the hadron calorimeter which provides 2 or more additional longitudinal samplings and full containment of the electromagnetic shower. The fine segmentation provided by the tower structure provides transverse sampling for additional rejective power against hadron contamination of the electromagnetic signals. We estimate that the π/e contamination for our detector will be less than 10^{-3} for an individual track.[12]

3) Hadron Calorimeter

The hadron calorimeter employs gas sampling in the saturated avalanche mode with pad readout as the preferred technique. This hadron calorimeter together with the electromagnetic calorimeter described in Section III.B.2 will have good detection efficiency and energy and angular resolution for hadrons as well as good tagging efficiency and angular resolution for muons. The good energy resolution is, in part, due to the scintillation properties of the scintillation glass. The good angular resolution is possible because of the excellent granularity of the gas sampling and will be discussed in detail in a later section. Finally the additional information from the extra longitudinal segmentation and sampling provided by the hadron calorimeter enhances the π/e rejection ability of the electromagnetic calorimeters.

These capabilities are essential in order to a) obtain maximum information on those events with interesting electromagnetic energy deposition ($e^{\pm}\gamma$, $e^{+}e^{-}$, $e^{+}e^{-}\gamma$, $e^{\pm}\nu$, $e^{\pm}$ jet) b) be able to completely analyze multihadron final states (multiple jet structure) c) identify leptons produced in the same direction as jets (weak decays of heavy flavors).

The hadron calorimeter, shown in Figs. 1a and 1b, like the electromagnetic calorimeter consists of three components. The central hadron calorimeter (CH) covers the region from 30° to 90° and is matched with the CEM in both tower segmentation and coverage. The CH is divided into 2 segments in depth and 10 orange slices in

azimuth. Each slice consists of 3 sections covering θ-ranges of 30°-60°, 60°-120°, 120°-150° as shown in Fig. 1a. Each section consists of alternating sheets of steel and gas-tube planes. A G10 board between each gas-tube plane and the adjacent steel plate contains the pads for readout.

The two forward hadron calorimeters (FH) cover the same angular regions as the FEM and are matched with the FEM tower structure. Each of these calorimeters is divided into 3 segments in depth and is split into 2 sections left and right of the beam.

Finally the two small very forward Fe/W hadron calorimeters (VFH) cover the small angle regions from 0.5° to 5° from the beam. Each of these calorimeters has a Pb/W electromagnetic front end (VFEM) which provides electromagnetic coverage down to small angles. These are a total of 5 segments in depth in the VFH. Tungsten is used because of its high density in both the VFH and the VFEM at angles less than 1.7° to minimize the extent of the apparatus along the beam to allow insertion of the low beta quadrupoles and to improve the p_T resolution by limiting shower size.

The pads of the gas sampling system define the tower structure of the hadron calorimeter and match with the tower structure of the electromagnetic calorimeter. Fine transverse segmentation provides advantages which have been demonstrated by several experiments (E609-Fermilab, UA2-CERN) and have been quantified in numerous studies.[23]

The transverse tower sizes and the tower distances from the interaction point are chosen to match several factors:

a) An affordable degree of segmentation with the desired angular resolution for the individual towers. A value for the pseudorapidity intervals of $\Delta\eta = 0.2$ is chosen to provide angular resolution fine enough to not appreciably worsen the p_T-resolution beyond the broadening due to the energy resolution (typically ± 10%). The $\Delta\eta = 0.2$ segmentation then fixes the tower θ-segmentation to $\Delta\theta/\theta = \pm 10\%$. The desire to keep the towers approximately square in transverse size fixes the ϕ-segmentation to $\Delta\phi = 12^{\circ}$.

b) The desired angular resolution with the hadronic shower size. The distance from interaction point, I, is then specified by requiring the tower size to be comparable with the typical dimensions of a hadronic shower. Since the position resolution of a hadronic shower is roughly 1/4 of its width, our θ-measurement uncertainty for a hadronic shower is $\Delta\theta/\theta \simeq \pm 5\%$.

To minimize detection inefficiencies and maximize detector structure simplicity, we limit our choice to 3 different radii and use slightly different $(\Delta\eta, \Delta\phi)$ segmentation in two regions:

a) In $\theta = 70^{\circ}$ to 110° we use $\Delta\eta = 0.1$ and $\Delta\phi = 6^{\circ}$, otherwise the segmentation becomes too coarse for containing a single hadronic shower.

b) At θ = 8 to 30 mrad, $\Delta\eta$ and $\Delta\phi$ are larger and determined by the smallest possible towers of 2.5 cm x 2.5 cm (made out of tungsten), effectively limited by the hadronic shower size.

These considerations produce about 1660 towers with almost half of them in the central region and the rest in the forward and very forward regions, listed in detail in Table IV.

Table V gives examples of tower transverse dimensions near the peak of the shower (1.5 a.l. in depth) for several θ's.

The towers at different angles will typically receive particles of different energies. The thicknesses of the towers have been chosen to give approximately similar fractional energy resolution over the full sphere, for the relevant particle energies. We expect an energy resolution of $70\%/\sqrt{E}$ to $100\%/\sqrt{E}$ for hadrons, and better than $\pm(8\text{-}10)\%$ for jets. The π^0's are measured much more accurately ($\pm 1\text{-}2\%$) by the e-m calorimeter.

In addition, we plan to record the hits

a) of individual wires in 10 different gas tube planes distributed along the full depth of each hadron calorimeter and the plane in the first e-m calorimeter gap.

b) of pads in 3 different planes inside the hadron calorimeters.

This will be very useful in combination with the information from the tracking chambers, calorimeter tower segments and the e-m gas sampling chamber pads in order to tag straight-through particles ($\mu, \pi^{\pm}$) traversing the whole length of the calorimeter and measure

accurately their position and to distinguish electrons/γ/π^0 from hadrons in the vicinity of showers. This could help us among other things to:

a) Associate a large amount of missing p_T in a given event with the presence of a non-interacting charged particle or perhaps an escaping ν (or photino).

b) Identify electrons in the vicinity of jets signaling possibly weak decays of heavy quark flavors.

IV. The Measurements

In order to quantify the physics capabilities of this detector, we have studied the questions of data rates, backgrounds and resolutions for those goals for which these quantities can be calculated. In order to calculate rates we have assumed, given the configuration of our spectrometer shown in Fig. 1, that an installation of low beta quadrupoles which would allow $\beta^* \sim$ 2 m is feasible. This β^* corresponds to a luminosity of 5×10^{29} cm^{-2}/sec at DØ for our detector. We have assumed that the collider will be operating with 1000 GeV $\bar{p}$ on 1000 GeV protons at the time of this experiment. We estimate 40000 interactions per second and are planning for beam crossings every 3.5 microseconds (a maximum of 6 bunches in the Collider). If a typical run of this detector is taken to be 10^7 seconds, (6 months at approximately 100 hours per week), we will accumulate an integrated luminosity of 4×10^{36} cm^{-2}. Under these assumptions we discuss some of our major physics objectives:

A. Study of $Z^o \to e^+e^-$

The extreme importance of the detection and precise measurement of the Z^o mass and width by measurement of its e^+e^- decay mode have been pointed out in many places.[2] The major objectives, once the observation of the Z^o is accomplished, are 1) to determine the existence of new neutrinos, leptons, or quarks by the precise measurement of its width, and 2) the determination of $\sin^2\theta_W$ by a high precision, systematics free measurement of the mass. In order to accomplish these two objectives reasonable statistics, high resolution and good control of systematics are required in our experiment.

Rates for Z^o production have been calculated using the zeroth order QCD Drell-Yan formalism,[23] the Weinberg-Salam SU2 × U1 couplings[2,24] of the quarks and leptons to the Z^o, and the CDHS nucleon structure functions.[25] The constituent interaction picture shown below

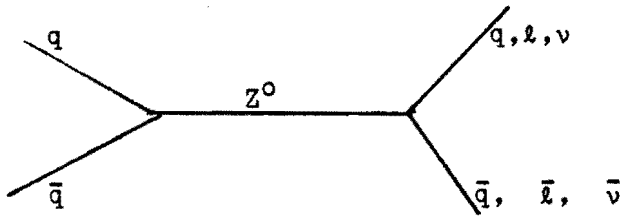

leads to the production cross section

$$\frac{d\sigma}{dX_F} = 2G\pi\sqrt{2}\,\frac{X_aX_b}{(X_F^2+4\tau)^{1/2}} \cdot \underbrace{\frac{1}{3}}_{\text{color factor}} \cdot \sum_{i}^{\text{quark flavors}} C_i[q_i(X_a)\bar{q}_i(X_b) + (a \leftrightarrow b)] \qquad (1)$$

where, as usual, $X_F = X_a - X_b$ and $\tau = M_z^2/S = X_aX_b$. C_i are the usual Weinberg-Salam functions of $\sin^2\theta_W$ which give the couplings of the various quark flavors to the Z^o. $q_i(X_a)$ are the quark structure functions of the nucleons and G is the Fermi constant. Just as the 'naive' Drell-Yan process for muon pair production is only the zeroth order QCD contribution to high mass pair production, this diagram gives only zeroth order contributions to Z boson production. We will need to multiply by a K factor[26] just as in the case of massive muon pair production to take into account the unknown contributions of higher order (in α_s) diagrams[27] such as

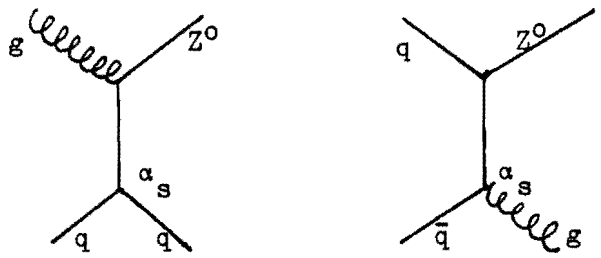

Compton Scattering Annihilation

These higher order processes will generate the p_T of the Z^o. We have assumed an arbitrary $e^{-p_T/5\ GeV/c}$ distribution for the purposes of Monte Carlo studies of the P-726 detector. Figure 4 shows the cross section as a function of X_F which we calculate from this simple picture of Z^o production using the CDHS quark structure functions for the proton and antiproton. No Q^2 evolution of these structure functions has been attempted in this calculation although $M_Z^2 = (\pi\alpha/G\sqrt{2})/(\sin^2\theta_W \cos^2\theta_W) \approx (88.6\ GeV/c^2)^2$ is quite far from $Q^2 \sim 200\ GeV^2/c^4$ region of the CDHS measurements. The total cross section obtained from this simple model is 4.4×10^{-33} cm^2 which gives a total production of Z^o for our assumed luminosity of 4×10^{36} of $\sim$ 18000 events. Using the e^+e^- branching ratio of 3.5% that is expected if there are only 6 weak doublets of masses less than $M_{Z^o}/2$ and using a K factor[28] = 2.3 to take into account higher order QCD production processes in $\bar{p}p$ interaction we obtain

$$\boxed{N_{Z^o} \approx 1500 \text{ events}} \quad \text{(6 month run)}$$

Using the production model discussed above and ignoring possible polarizations of the Z^o, we have studied the measurement of the Z^o width. Both the energy resolution of the scintillation glass electromagnetic detector and the angular resolution achievable with the central and forward tracking

chambers have been taken into account in estimating the mass resolution of the P-726 detector. Based on the E-705 test measurements[11] and studies with the EGS[29] shower Monte Carlo we believe that a resolution of $\Delta E/E \backsim 0.7\% + 1.1\%/\sqrt{E}$ can be achieved and maintained by this device. For the $Z^0 \rightarrow e^+e^-$ decay because of the large light yield of the glass due to the large energies of the decay products ($e^{\pm}$), the systematic contribution to the energy resolution is much larger than the photon statistics contribution. This is indicated in Fig. 5 by the superposition of the photon statistics contribution to the photon energy resolution on the expected energy spectrum of electrons from Z^0 decay. Therefore, the stability of the detector that is made possible by the use of photodiodes and the radiation immunity of the scintillation glass is critical. The angular resolution due to the tracking chamber measurement error is a negligible contribution to the measurement error of the mass. The various contributions to the mass resolution estimated by Monte Carlo studies of the apparatus are:

	Scintillation Glass
σ_1 (electron angular resolution)	= 125 MeV/c^2
σ_2 (electron energy-photon statistics)	= 110 MeV/c^2 ($1.1\%/\sqrt{E}$)
σ_3 (electron energy-systematics)	= 450 MeV/c^2 (0.7%)
σ_{total}	= 530 MeV/c^2

The total resolution is not exactly the sum in quadrature of the components because of correlations.

The natural width of the Z^0 for 6 doublets is calculated to be $\sim$ 2200 MeV/c^2. The partial widths for each new neutrino, lepton, and quark are

$$\Gamma(Z^0 \to \ell^+\ell^-) \sim 77 \text{ MeV}/c^2$$
$$\Gamma(Z^0 \to \nu\bar{\nu}) \sim 144 \text{ MeV}/c^2$$
$$\Gamma(Z^0 \to q\bar{q}) \sim 604 \text{ MeV}/c^2$$

corresponding to changes in the natural width of 3.5%, 7.0%, and 27.5% respectively. We may expect with 1500 events to be able to measure the width Γ to an accuracy

$$\Delta\Gamma \sim \left(\frac{2}{N}\right)^{1/2} \cdot \sqrt{\Gamma^2_{\text{Natural}} + \text{FWHM}^2 \text{ (measurement error)}}$$

$$= 3.7\% \sqrt{(2200 \text{ MeV}/c^2)^2 + (1248 \text{ MeV}/c^2)^2}$$

$$\sim 93 \text{ MeV}/c^2$$

Note that if the detector had perfect resolution, the statistics would be sufficient to perform the measurements to 80 MeV/c^2. We, therefore, expect to be able to see new quark flavors readily. Considerably more statistics would be required to attempt the search for new neutrinos by this method.

B. Study of Quarkonium States $\to e^+e^-$ and $e^+e^-\gamma$

The detection and measurement of the production of $q\bar{q}$ bound states of heavy quarks ($c\bar{c}$, $b\bar{b}$, $t\bar{t}$, etc.) via their e^+e^- and $e^+e^-\gamma$ decay modes is an important capability of the P-726 detector. In particular the detection of the top quark by searching for the s states of the $t\bar{t}$ system at masses higher than 45 GeV (PETRA's expected peak energy) with the best possible resolution

for the e^+e^- decay mode is a major goal of this experiment. In addition, the study of the hadronic production of lighter quark-antiquark states (such as charmonium and upsilonium which have been detected at lower energies[31,32]) will be easier because of the increased production cross sections at collider energies.

Because of the excellent electromagnetic mass resolution for e^+e^- final states ($\sigma \sim 450 \rightarrow 550$ MeV/c^2) the P-726 detector should have better sensitivity for detection of the e^+e^- from toponium decay than other proposed detectors. The small cross sections and low expected yields of the 1 S ground state in $\bar{p}p$ collisions at $\sqrt{s} = 2000$ GeV put a premium on the stability and resolution of the detector. We show below the event yields and the Drell-Yan backgrounds as a function of $t\bar{t}$ mass expected for a 4×10^{36} cm^{-2} integrated luminosity run.

$t\bar{t}$ Mass ($\Gamma \sim 5$ KeV)	$\sigma \cdot B(t\bar{t} \rightarrow e^+e^-)$ Ref. 4	Number of events	Drell-Yan Background
40 GeV/c^2	1.3×10^{-35} cm^2	52	2.0
50 GeV/c^2	7.5×10^{-36} cm^2	30	0.6
60 GeV/c^2	1.5×10^{-36} cm^2	6	0.3

During the approximately 6 months that the experiment will operate, large numbers of $c\bar{c}(J/\psi)$ and $b\bar{b}(T)$ bound states will be produced and detected via their e^+e^- decay modes. We have extrapolated the cross sections for ψ and T measured at lower energies using the $B \cdot \sigma \sim \bar{e}^{\alpha\sqrt{\tau}}$ form for the τ-behavior for ψ and T production.[33,34] We predict the following numbers of T and ψ in a 6 month experiment.

Resonance	Number of Events
$J/\psi \rightarrow e^+e^-$	$\sim$ 200,000
$T \rightarrow e^+e^-$	$\sim$ 2,000

As has been the case[35] in the $c\bar{c}$ charmonium and the $b\bar{b}$ upsilonium system, a complex level structure of s and p states is expected in the $t\bar{t}$ toponium system. The near identity of the charmonium and upsilonium s state spectra has led to the hypothesis that the $q\bar{q}$ potential in the 0.1 to 1 fermi region probed by the heavy quarks has a logarithmic form.[3] This leads to the expectation that the s and p states of toponium would have similar level structure with perhaps a small increase in the spacing of levels. Since the number of s state events which are produced are expected to be small and since there will be interest in the detection of the p states structure in any case, a premium will be placed on a detector which can measure the expected radiative transitions between states. The production of the p states can occur directly in a hadronic interaction whereas in e^+e^- collisions the p states appear only as products of the decay of higher s states. Therefore, some of the spectroscopy of quarkonium system and certainly the study of hadronic production of quarkonium may be unique to hadronic colliders.

While the number of toponium p states which can be produced in this experiment is uncertain because of unknown production cross sections and branching ratios of the radiative decays, the experimental observation[32] in the charmonium has been that 36% of the (J/ψ)'s produced in hadronic interactions come from radiative decays of p states. If the situation is analogous in the toponium system, we may expect a few tens of toponium p

states decaying into $e^+e^-\gamma$. During the same run we may expect to see 70,000 charmonium and 700 upsilonium p states produced and decaying into $e^+e^-\gamma$. In the p state center of mass the photon energies will be of order 500 MeV if the theoretical speculation is correct. With a reasonable production model for the toponium p states, the laboratory energy spectrum of the photons from p state decay will be as shown in Fig. 6. Similar spectra will result from charmonium and upsilonium p state decays since these photons are also approximately 500 MeV. A considerable portion of the photon energy spectrum still lies in the region where the photon statistics of the electromagnetic detector dominates the resolution (note the resolution curves of lead and scintillator glass in Fig. 6). The small spacings of the p states (which are as small as 40 MeV in the case of charmonium) will require good energy resolution if we are to resolve them. Using the expected energy resolution of our electromagnetic detector and reconstructing the electrons in the tracking chambers we have estimated the mass resolution of the detector. We have also used the mass of the 1 s state as a constraint on the calculation. In the absence of any considerations of electronic amplifier noise (see Appendix B), we estimate a mass resolution of $\sigma \backsim 10$ MeV/c^2 using this technique (compared with approximately 30 MeV/c^2 that can be achieved with lead glass assuming the same level of systematics, 0.7%). This excellent resolution will be more than adequate to resolve the quarkonium states with separation of 100 MeV/c and will greatly aid any search for toponium p states. However, the achievement of this level of resolution may require the use of vacuum phototriodes with an amplification of $\backsim 10$ (Appendix B). An optimistic analysis of the electronics of the scintillation glass-photodiode system gives an electronic noise

equivalent to 40-50 MeV. This noise level increases the energy resolution by 20% for a 3 GeV photon and degrades the p states mass resolution to $\sigma \sim 25$ MeV/c^2. More pessimistic estimates of our electronic noise would lead to 80-100 MeV levels, thereby making vacuum phototriodes very desirable in order to recover the resolution curves of Fig. 6. Suitable vacuum triodes have been developed[40] but, to date, have not been adequately packaged in a configuration thin enough to allow use in the shell structure shown in Fig. 1b without increasing slightly the overall dimensions of the detector.

The levels of combinatorial background that we might experience in a search for p states has been only crudely estimated at this time. This background is produced by the many photons in the final state of every interaction which contains a true 1 s ground state of a given type of quarkonium. Estimating 10-15 π^0's in the $\sqrt{s}$ = 2000 final state of which a portion will fail to be reconstructed, we might find 10-15 $t\bar{t}\gamma$ combinations which could form a background for a p state search. However, these combinations will, in general, have a fairly uniform mass distribution. We estimate that we would have less than 1 in the 1 GeV/c^2 mass interval above the 1 s ground state per event. We might guess that 1/3 of all 1 s states comes from decay of p states. With the 15 MeV/c^2 mass resolution, this corresponds to less than 20% background for any peak search.

C. Detection and Measurement of Final States with Missing p_T

The utility of measuring missing p_T at colliding detectors has been well demonstrated at CERN where the missing p_T measured was crucial in identifying the decay of the W and in specifying its mass. We know that this technique

will be useful at the Tevatron in further exploring "known" physics such as the $W^{\pm}$ and Z^{o}. We are also convinced that this technique will be indispensable in our search for new and "unknown" physics at the new energies, a search for which we have no reliable guidance. To perform this kind of measurement with any sensitivity, a detector must have a number of capabilities. These include:

a) The ability to perform calorimetric energy measurements over the whole 4π solid angle in order to minimize the maximum possible escaping p_T.

b) The capability of good hadronic and electromagnetic calorimetric measurements. We note that the resolution in p_T is largely determined by the resolution of the hadronic calorimetry. In our case, the calorimeter is designed with a hadronic energy resolution of $70\%/\sqrt{E}$ to $100\%/\sqrt{E}$ (depending on angle of the hadron).

c) The ability to easily identify and separate both individual particles and particle jets. This argues strongly for a detector geometry based on a fine segmentation with towers, pointing back to the interaction vertex.

As described in Section III, we have designed our apparatus with these considerations firmly in mind.

Since the detector has no magnetic field, non-interacting tracks carry away an unknown amount of p_T. Events with such tracks must be tagged. If this sort of measurement is to be practical, the fraction of such events must be small. We can estimate a good upper limit to this number by considering the two major sources of penetrating tracks, muons from decaying pions and kaons,

and punch-through hadrons, following the work of Ascoli.[36] Our central detector, in this respect, has an advantage over CDF in having a smaller inner radius (60 cm vs. 170 cm) thus having a shorter decay path, and a disadvantage in having less absorber in the central region (5 absorption lengths vs. 6.4 near 90^{o}). The problem is much less serious in the forward direction because of increasing amounts of absorber and higher average momenta. The two effects tend to nearly cancel and we arrive at conclusions similar to those of CDF: at small p_T (10 GeV/c) the decay contribution dominates but at larger p_T (40 GeV/c) punch-through has grown to the point where both effects contribute nearly equally. The integral background is less than 10^{-28} cm^2 or about 10^{-3} of the total interaction rate. The distribution of escaping particles has a very steep fall-off in p_T, dropping by 4-6 orders of magnitude for p_T greater than 10 GeV/c. This will be an important consideration in triggering the apparatus in a conceivable measurement that we discuss below.

If the theoretical conjectures based on supersymmetry are verified experimentally, and if the mass scale falls in the range accessible to experiments at the Tevatron, then a measurement of missing p_T could yield information about the new energy regime not possible by any other technique. Detailed calculations of the detection of "gluinos" by calorimetric technique have been made by Aronson, et al.[5] A curve, taken from their paper, showing the signal for various mass gluinos along with the backgrounds contributed by light quark semileptonic decays produced in $\sqrt{s}$ = 800 GeV collisions is shown in Fig. 7. The utility of good electron and muon identification is underscored by the realization that the background may be suppressed by identifying and discarding events with leptons of substantial energy since

generally speaking gluino events would not contain them. If we assume that the cross section scales in $\tau = m^2/s$, then we estimate that at the Tevatron, in our standard running period, we would observe about 2000 gluinos with a mass of 75 GeV/c^2 above a background typically a factor of four to six lower.

Appendix A

Properties of Scintillation Glass (SCG1-C)

A new heavy glass has recently been developed for use in electromagnetic shower counters for high energy physics which differs in both composition and operation from the lead glasses which have been used for the last decade for this purpose. The proposed P-726 detector makes use of this scintillation glass because of the several advantages that it has over lead glass. These are:

a) Better energy resolution.

b) Higher output light level for a given shower making possible use of photodiodes.

c) Much more immunity to radiation damage.

d) A large component of light output is scintillation light from dE/dX loss rather than Cerenkov light thereby making it much more suitable for use in front of a hadron calorimeter.

The purpose of this appendix is to briefly summarize the properties of scintillation glass (the SCG1-C glass available from Ohara Optical) and to contrast these properties where appropriate to the more familiar SF5 lead glass.

In general the scintillation glasses thus far developed have as their heavy component BaO. In addition they contain some oxide of Cerium which produces both scintillation light directly from dE/dX and acts as a wavelength shifter of Cerenkov light. So there are three components of the light output from a given shower, direct scintillation light, direct Cerenkov light, and wavelength shifted Cerenkov light. The relative properties of SCG1 scintillation glass and SF5 lead glass are given below:

	Scintillation Glass (SCG1-C)	Lead Glass (SF5)
Composition (by weight)	SiO_2 - 42.5% BaO - 43.4% MgO - 3.3% Li_2O - 4.0% K_2O - 3.3% AI_2O_3 - 2.0% Ce_2O_3 - 1.5%	SiO_2 - 38% PbO - 55% K_2O - 5% Na_2O - 1%
Radiation Length	4.35 cm	2.54 cm
Nuclear Absorption Length	45.6 cm	42.0 cm
Speed	C - Fast Comp $\sim$ 2 ns Scint - Slow Comp $\sim e^{-t/70ns}$	C $\sim$ 2 ns
Density	3.36 gm/cm^3	4.08 gm/cm^3
Index of Refraction	1.603	1.67270
Excitation Wavelength	375 n meters	-
Fluorescent Wavelength	429 n meters	-
Photon Statistics contribution to resolution σ/E (Refs. 11,12,13)	$\frac{1.13 \pm 0.33\%}{\sqrt{E}}$	$\frac{4.3\%}{\sqrt{E}}$
Light output* relative to SF5 Lead Glass (Refs. 11,15,37)	5.1 ± 0.3 5.0 4.5	1

Light Production Mechanisms	1) Direct Ĉ 2) Wavelength shifted ĉ 3) Direct Scintillation Light		Direct Ĉ
Transmission		1 cm	26.1 cm (6 rl)
	390 nm	94.52%	23.0%
	420 nm	99.74%	93.4%
	500 nm	99.94%	98.5%

		1 cm	15.2cm (6 rl)
	390 nm	96.72%	60.2%
	420 nm	98.99%	85.7%
	500 nm	99.60%	94.1%

		10^{10} GeV/cm^2 (extrapolated)	10^{12} GeV/cm^2	10^{10} GeV/cm^2	10^{12} GeV/cm^2 (extrapolated)
Radiation** Damage Quantified	436 nm	97%	34%	42%	
	546 nm	99.7%	88%	59%	Completely
	570 nm	~100%	95%	65%	black

Cost (Ref. 38)	\$0.189/cm^3 (\$0.82/cm^2•rl)	\$0.185/cm^2 (\$0.47/cm^2•rl)

* To interpret this number the geometry of the individual counters and the various experimental setups in the references 11,15,37 must be examined.

** This measurement of radiation damage was performed using 90 MeV protons and the decrease in transmission was measured along the direction of the incident beam. The actual damage due to high energy showers may be considerably different but we assume that the decrease in transmission along the axis of the shower will still be proportional to the energy deposited per cm^2 in the glass.

Appendix B

Vacuum Photodiodes

Over the past 2 or 3 years, vacuum photodiodes have come to be considered strongly as readout devices for calorimeters either in sampling calorimeters[16] or in fully-active calorimeters using NaI or similar material.[39] Over a wide range of energies and module sizes, one finds that large enough numbers of signal photoelectrons can be obtained so as to make amplifier noise unimportant with the use of inexpensive low-noise charge-sensitive amplifiers[40], operated at rise times of 50 to 200 nanoseconds.

The Pennsylvania group has developed, with the Hamamatsu Corporation, a new type of flat vacuum photodiode, for calorimeter use, and has built and tested a prototype e-m sampling calorimeter using such diodes.[17] We plan to use such photodiodes to read out the scintillating glass in our proposed e-m calorimeter. The major advantages of photodiodes in this application, as compared to photomultipliers, are:

1. Gain stability -- the "gain" is unity.
2. Minimal thickness, permitting efficient tower construction.
3. Ready adaptability to segmenting, using "pads" in the diodes.
4. No need for high voltages or highly stabilized voltages.
5. Reduced requirements on calibration and monitoring systems.

Gain stability is of prime importance. For high-mass e^+e^- pairs, the P-726 e-m detector has a mass resolution limited not by photoelectron statistics or by amplifier noise, but instead purely by gain stability and by systematics. This will be true for e^+e^- masses greater than 5 or 10 GeV--for

larger masses, the mass resolution is expected to be approximately 500 MeV/c^2. To operate a system of 1000 or 2000 photomultipliers (the number we would need) under conditions which could give short-term and long-term stability better than 1% would require a level of performance superior to any that has been achieved to our knowledge. With photodiode readout, however, we expect gain stability of this quality to be relatively easy to obtain. Finally, the minimal thickness of the diodes and their high segmentation flexibility are important for improved performance, simplicity and lower overall detector cost.

The use of photodiodes and amplifiers in our detector require that we estimate the electronic noise of the system. We expect with coverage of the surface area that can be achieved with the photodiodes and the level of photon statistics that has been observed (see Appendix A) that we will have $\sim$ 12000 photoelectrons/GeV of energy. Amplifier systems have been designed, built and measured by R. Boie and V. Radeka[40] at BNL for use with the calorimetry of CERN experiment R807. The noise level measured was approximately $\sigma \sim 500$ electrons for a source capacitance of 20 pf and amplifier shaping time of 500 ns. If we use an amplifier shaping time of 2 μs and a multiple parallel FET input stage to each amplifier, it may be possible to limit the amplifier noise contribution to the total energy resolution to 40 MeV even with the multiple amplifier summation that is required. More realistically we may expect a degradation of a factor of $\sim$2 to the 80 MeV level.

This troublesome electronic noise component can be eliminated if a small amount of gain can be achieved. Vacuum triodes have been developed and successfully tested by M.D. Rousseau and collaborators[41] at Rutherford Laboratory and a gain of 10 has been achieved. We can eliminate the amplifier

noise problem by use of this device without sacrificing stability. At this point no suitable packaging has been developed that is thin enough to be directly usable in our detector, but we see no insurmountable problems with achieving such packaging.

Appendix C

Cost Estimates

A preliminary cost estimate has been made for each of the parts of the P-726 detector. Many uncertainties are incorporated in these estimates. We present these costs in several ways. In Table VI we have presented a breakdown of the costs by function, i.e., tracking electromagnetic and hadron calorimeter so that the cost of each capability of the detector may be ascertained. Table VII presents a slightly different viewpoint, where we have costed separately the CEM, CH, FEM, FH, FVEM, and VFH parts of the detector (indicated in Fig. 1) so that the cost of each type of angular coverage can be factored.

These estimates have been prepared based on the experiences of various experiments (E-395/E-609, E-537/E-705, E-594) and from private communications with M. Atac and M. Mishina of the CDF collaboration. In addition extensive communication have been underway between the proponents of P-726 and Ohara Glass Ltd and Hamamatsu Co.

REFERENCES

1. H. Gordon, et. al., "Testing the Standard Model," Snowmass (1982).

2. C. Quigg, Reviews of Modern Physics, Vol. 49, No. 2, 297 (1977).

3. P. Moxhay, J. L. Rosner, and C. Quigg, Physical Review D, 23, 2638 (1981).

4. J. D. Jackson, S. Olsen, and S. H. H. Tye, "Properties of Toponium," Snowmass (1982).

5. S. H. Aronson, et. al., BNL 31885 (1982).
G. L Kane and J. P. Leveille, Physics Letters, 112B, 227 (1982).

6. I. Hinchliffe and L. Littenberg, "Phenomenological Consequences of Supersymmetry," Snowmass (1982).

7. K. Lane, "The Scalar Sector of the Electroweak Interaction," Snowmass (1982).

8. G. Arnison, et. al., CERN-EP/83-13 (1983).

9. Design Report - Tevatron I Project, October (1982).

10. G. Arnison, et. al., Physics Letters, 118B, 167 (1982).

11. B. Cox, et. al., Fermilab - Conf. - 82/75 EXP, to be published in the proceedings of the Nuclear Science Symposium, Washington D. C., October (1982).

12. J. A. Appel, et. al., Nuclear Instruments and Methods, 127, 495 (1975).

13. J. E. Brau, et. al., Nuclear Instruments and Methods, 196, 403 (1982).

14. Private communication, E-705 collaboration.

15. M. Kobayashi, et. al., KEK Preprint 81-8 (1981).

16. W. Kononenko, et. al., Nuclear Instruments and Methods, 186, 585 (1981).

17. W. Kononenko, et. al., to be published in the proceedings of the Nuclear Science Symposium, Washington, D. C., October (1982).

18. M. Atac, et. al., FNAL Workshop on Gas Calorimetry, October (1982).

19. D. Bridges, et. al., Contribution to the International Conference on Experimentation at LEP, June (1981), Physica Scripta 23, 655 (1981).

20. M. Banner, et. al., UA2 Collaboration, CERN/SPS/78-08 and CERN/SPS/78-54 (1978).

21. W. Farr, et. al., Nuclear Instruments and Methods, 156, 283 (1977).

22. B. Cox, et. al., Fermilab - Conf. - 82/76 - EXP, to be published in the proceedings of the Nuclear Science Symposium, Washington, D. C., October (1982).

23. Design Report for the Collider Detector Facility, 49 (1981).

24. S. D. Drell and T-M Yan, Physical Review Letters, 25, 316 (1970).

25. S. Weinberg, Physical Review Letters 19, 1264 (1967).
S. Weinberg, Physical Review Letters 27, 1688 (1971).
A. Salam, Elementary Particle Theory: Relativistic Groups and Analyticity (Nobel Symposium No. 8), 367 (1968).
S. L. Glashow, J. Iliopoulos, and L. Maiani, Physics Review D2, 1285 (1970).

26. J. G. H. de Groot, et. al., CDHS collaboration, Physics Letters, 82B, 456 (1979).

27. B. Cox, Rapporteur Talk, Proceedings of the XXI International Conference on High Energy Physics, Paris, France (1982).

28. G. Altarelli, G. Parisi, R. Petronzio, Physics Letters, 76B, 356 (1978).

29. E. Anassontzis, et. al., Fermilab - Conf. - 82/50 - EXP (1982).

30. R. L. Ford and W. R. Nelson, SLAC - 210 (1978).

31. T. B. W. Kirk, et. al., Physical Review Letters, 42, 619 (1979).

32. Y. Lamoigne, et. al., Physics Letters, 113B, 509 (1982).

33. J. Badier, et. al., Physics Letters, 86B, 98 (1979).

34. L. Lyons, "Massive Lepton Pair Production in Hadronic Interactions and the Quarn Model," Progress in Particle and Nuclear Physics.

35. See Review of Particle Properties, Reviews of Modern Physics, Vol. 52, No. 2, 5154 (1980).

36. G. Ascoli, "Muon Detection for the Colliding Beam Experiment," CDF Note 57.

37. S. Bartalucci, et. al., Frascatti Preprint, LNF - 80/10 (P) (1980).

38. P. Brockington, Ohara Optical, private communication.

39. W. Willis, CERN Experiment R807, private communication.

40. R. Boie and V. Radeka, BNL, private communication.

41. M. D. Rousseau, private communication.

Table I

Planar Chamber Parameters

A) readout
   1) proportional sense wires all planes
   2) cathode pads, last plane of each region

B) wire plane configuration
   1) 4 planes/module
   2) sense wire orientation/module 0^o, 45^o, 90^o, 135^o
   3) modules/region: a) TC2: 10 (2 X 5)
      b) TC3: 6 (2 X 3)
      c) TC4: 10 (2 X 5)
   4) radii of planes a) TC2: 32.5 - 79.0 cm
      b) TC3: 21.5 - 25.0 cm
      c) TC4: 36.0 - 43.0 cm
   5) distance from center of intersection region
      a) TC2: 57. - 137. cm
      b) TC3: 250. - 290. cm
      c) TC4: 400. - 480. cm
   6) θ range covered
      a) TC2: 2.5^o - 30^o, 150^o - 177.5^o
      b) TC3: 1.2^o - 5^o, 175^o - 178.8^o
      c) TC4: 0.7^o - 5^o, 175^o - 179.3^o

C) cathode pad configuration
   1) last plane of each region
   2) average pad size = 1 cm^2
   3) cover an annular area of radii 6 cm to 20 cm
   4) θ range covered
      a) TC2: 2.5^o - 8.5^o, 171.5^o - 177.5^o
      b) TC3: 1.2^o - 4.0^o, 176^o - 178.8^o
      c) TC4: 0.7^o - 2.4^o, 177.6^o - 179.3^o

D) gap width 6 mm
E) sense wire pitch 2 mm
F) resolution/track/module $\sigma(X) = \sigma(Y) = .5$ mm
G) total number of planes 104
H) total number of wires 38000
I) total # cathode pads 7500

Table II

Cylindrical Chamber Parameters

A) Cylindrical Proportional Wire Chambers

1)	gap width	6 mm
2)	sense wire pitch	2 mm
3)	readout	sense wire & cathode strip pulse height
4)	total # readout channels	6573
5)	resolution/track/plane	σ (R$x\phi$) = .6 mm
		σ (z) = .3 mm

6) individual chamber parameters:

				cathode			
					helical		
chamber	radius (cm)	length (cm)	wires	rings	sections	strips/ section	total # strips
1	17	110	534	220	4	151	604
2	20	110	628	220	4	178	712
3	32	90	1005	180	2	284	568
4	35	90	1100	180	2	311	622
Total			3267	800			2506

B) Cylindrical Drift Chamber

1)	number of drift cells	60
2)	ϕ coverage/cell	6^{o}
3)	number of wires/cell	8
4)	total number of sense wires	480
5)	radial location of wires	22.5 through 29.5 cm, 1 cm spacing
6)	readout mode	drift time & charge division
7)	resolution/track/wire	σ(R$x\phi$) = .3 mm
		σ(z) = 10. mm
8)	number of readout channels	960

Table III

Summary of the Properties of the Electromagnetic Detectors

Properties	Central EM (CEM)	Forward EM (FEM)	Very Forward EM (VFEM)
Polar Angle (θ) Coverage	30°-90°	5°-30°	0.5°-5°
Number of Absorption Lengths	2	2	1
Number of Radiation Lengths	20	20	25
Material	SCG1-C glass	SCG1-C glass	Pb, W
Number of Longitudinal Segments	3	3	2
Number of Sampling Cells	3	3	25
Thickness of Longitudinal Segments	17.4, 26.1 43.5 cm	17.4, 26.1 43.5 cm	25, 20 cm
Thickness of Absorber Per Cell	-	-	0.6, 0.3 cm
Radial Distance from Detector Center of Detector Element	60 cm	150 cm	470 cm
Calorimeter Thickness	$\sim$95 cm	$\sim$95 cm	50, 40 cm
Volume	10 m^3	6 m^3	1 m^3
Weight	34 tons	20 tons	2 tons
Area of Diode or Gas Tube Coverage	37 m^2 (diode)	21 m^2 (diode)	29 m^2 (gas tubes)
Width and Number of Pseudo-rapidity (η) Intervals	0.2/14	0.2/14	0.2-0.6/18
Width and Number of Azimuthal Intervals	12°/30	12°/30	12°-60°/30-6
Number of Towers	420	420	460
Number of Readout Channels	1260	1260	920

Table IV

Summary of the Properties of the Hadron Calorimeter

Properties	Central Hadron (CH)	Forward Hadron (FH)	Very Forward Hadron (VFH)
Polar Angle (θ) Coverage	30°-90°	5°-30°	0.5°-5°
Number of Absorption Lengths (a.l.)	3	6	8
Material	Fe	Fe	Fe, W
Number of Segments	2	3	3
Number of Sampling Cells	19	26	26
Thickness of Absorber per Cell	2.5 cm	3.8 cm	5.1, 3 cm
Radial Distance from Detector Center of Detector Element	150 cm	250 cm	520 cm
Calorimeter Thickness	80 cm	140 cm	180, 110 cm
Volume	31 m^3	24 m^3	3 m^3
Weight	150 tons	130 tons	18 tons
Area of Gas Tube Coverage	720 m^2	435 m^2	45 m^2
Width and Number of Pseuod-rapidity (η) Intervals	0.1-0.2/18	0.2/14	0.2-0.6/18
Width and Number of Azimuthal Intervals	6°-12°/60-30	12°/30	12°-60°/30-6
Number of Towers	780	420	460
Number of Readout Channels	1560	1260	1380

Table V

Transverse Tower Dimensions

at 1.5 Absorption Length

Polar Angle θ	Size
10^{o}	13 X 13 cm^2
15^{o}	20 X 20 cm^2
20^{o}	27 X 27 cm^2
30^{o}	13 X 13 cm^2
40^{o}	17 X 17 cm^2
50^{o}	21 X 21 cm^2

Table VI

Detector Cost by Function

A.	Tracking System	
	1) Central Chambers	$250K
	2) Forward Chambers	$250K
	3) Chamber Electronics	$700K
B.	EM Calorimeters	
	1) Scintillating Glass (SCG1-C) (2528 blocks, 54 tons)	$3000K
	2) Vacuum photodiodes ($57.7\ m^2$ area)	$450K
	3) Photodiode Readout Electronics (Amplifiers + ADC's; 3400 channels)	$130K
	4) Sampling Chambers & Electronics (11000 channels)	$250K
C.	Hadron Calorimeters	
	1) Steel Plates (300 tons)	$300K
	2) Gas Sampling System ($1231\ m^2$ area)	$1600K
	3) Pad-tower Readout Electronics (4200 channels)	$170K
	4) Wire & Pad Sampling Electronics (35000 channels)	$350K
D.	Detector Mechanical Assembly	$500K
E.	Calibration + Monitoring	$150K

TOTAL COST = $8.1 M

Table VII

Detector Cost by Subdetector Section

1.	Central Tracking Chambers + em Calorimeter (CEM) (30° - 150°)	\$3.1 M
2.	Central Hadron Calorimeters (CH) (30° - 150°)	\$1.5 M
3.	Forward Tracking Chambers + em Calorimeters (FEM) (5° - 30°, 150° - 175°)	\$2.0 M
4.	Forward Hadron Calorimeters (FH) (5° - 30°, 150° - 175°)	\$1.0 M
5.	Very Forward Tracking Chambers + Calorimeters (VFH/EM) (8 - 80 mrad)	\$0.5 M
		\$8.1 M

FIGURE CAPTIONS

Figure 1a P726 4π nonmagnetic detector.
1b Expanded view of P-726 detector.

Figure 2a Central tracking chambers - section through center of intersection region parallel to beam axis.
2b Central tracking chambers - section through center of intersection region perpendicular to beam axis.

Figure 3 Schematic of the sense elements of the central PWC's. One section of helical strips removed. Gap width and electrode spacing expanded for clarity.

Figure 4 X_F distribution of Z^o production. CDHS structure functions used in calculations.

Figure 5 Energy spectrum of $e^{\pm}$ from $Z^o \rightarrow e^+e^-$ decay. The curves are the photon statistics and systematic contributions to the electron energy resolution.

Figure 6 Energy spectrum of photons from toponium decay to the 1s state plus a photon. The curves are the photon statistics and systematics contributions to the photon energy resolution.

Figure 7 Gluino production cross sections as a function of mass at $\sqrt{s} = 800$ Gev.

Figure 8a Radiation damage measured as a decrease in transmission for SF5 lead glass.
8b Radiation damage measured as a decrease in transmission for SCG1-C scintillation glass.

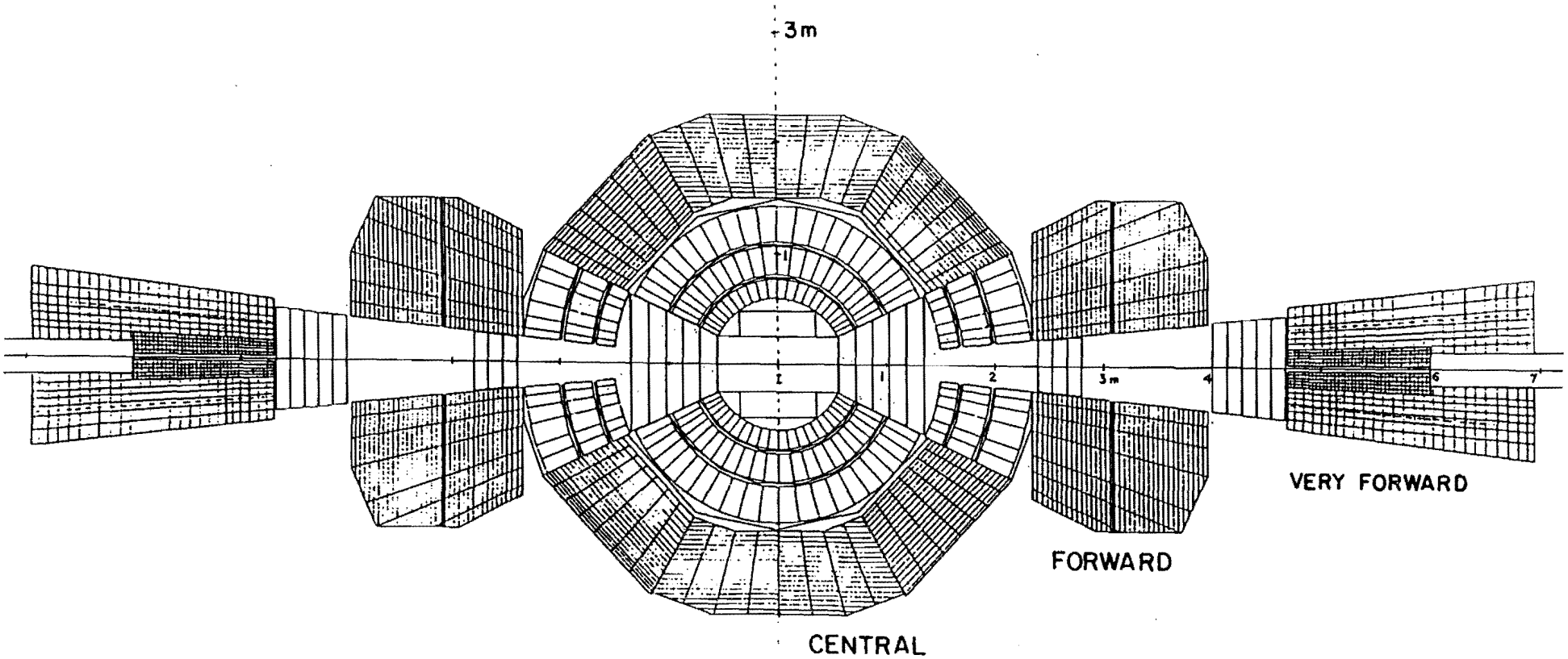
3m
1
1
2
3m
4
6
7
VERY FORWARD
FORWARD
CENTRAL
D0 - P726
JAN 30 1983

FIGURE 1a

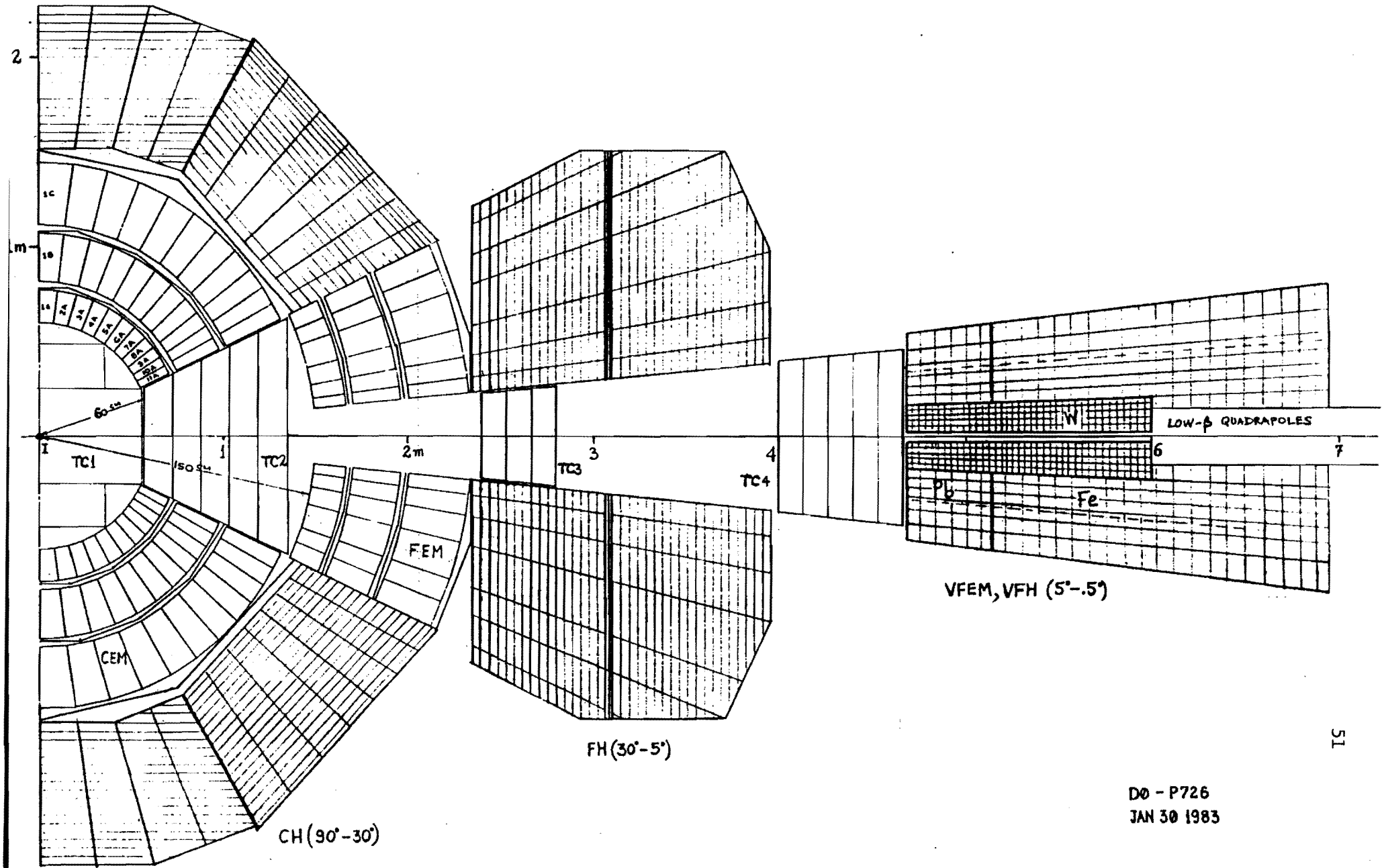

FIG. 1b.

DØ - P726
JAN 30 1983

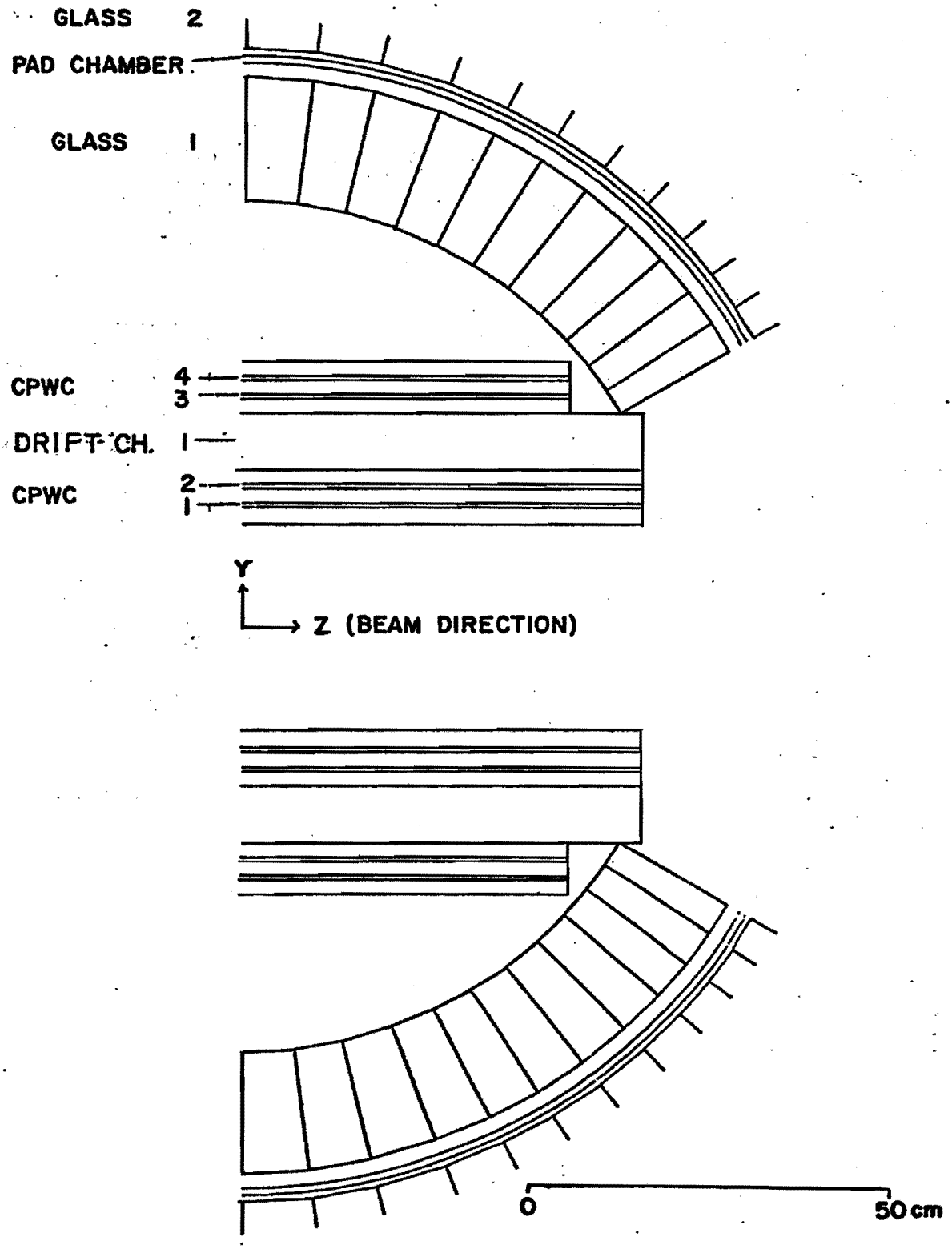

CENTRAL DETECTOR REGION
LONGITUDINAL SECTION
FIGURE 2a

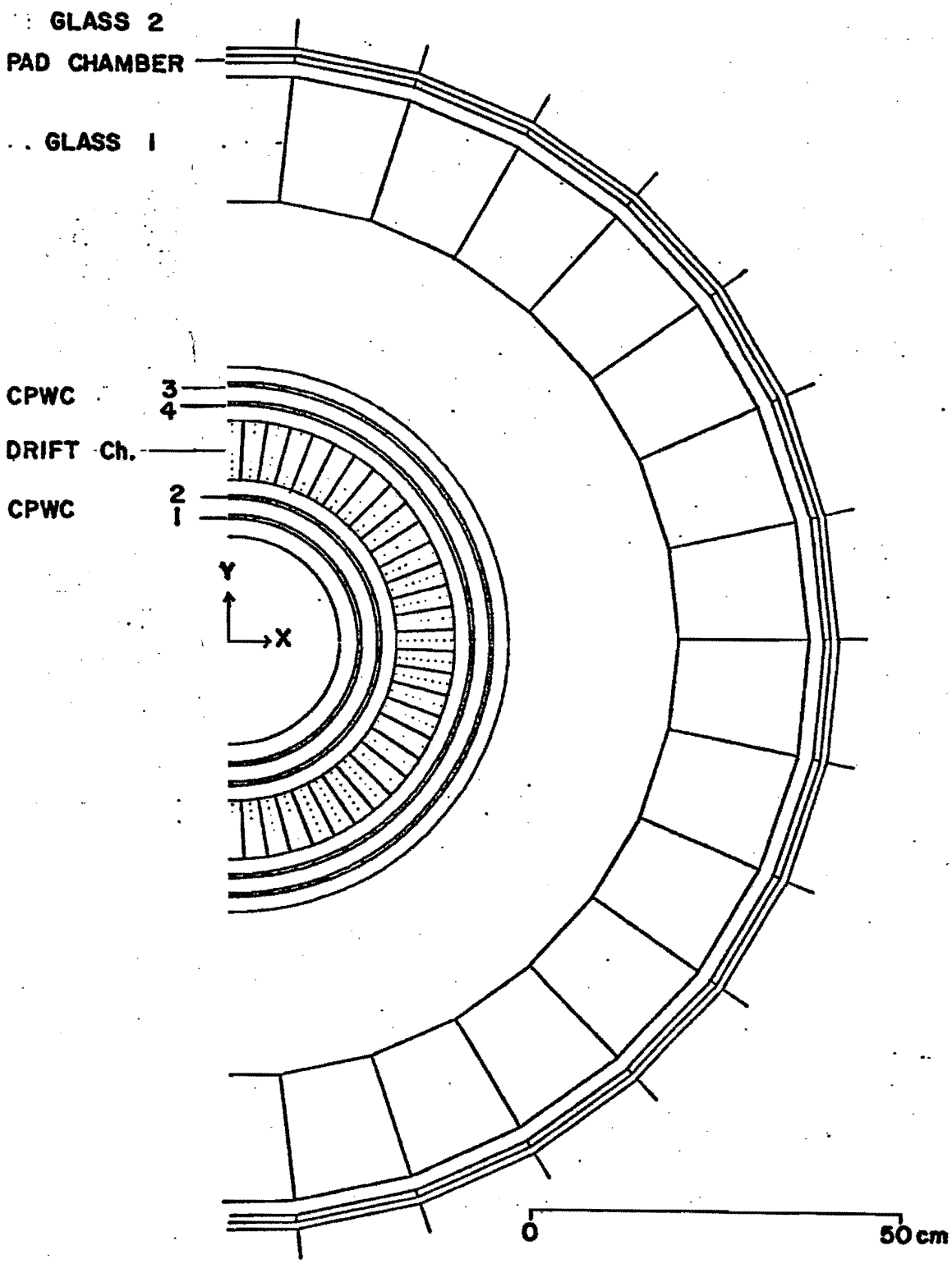

CENTRAL DETECTOR REGION
TRANSVERSE SECTION
FIGURE 2b

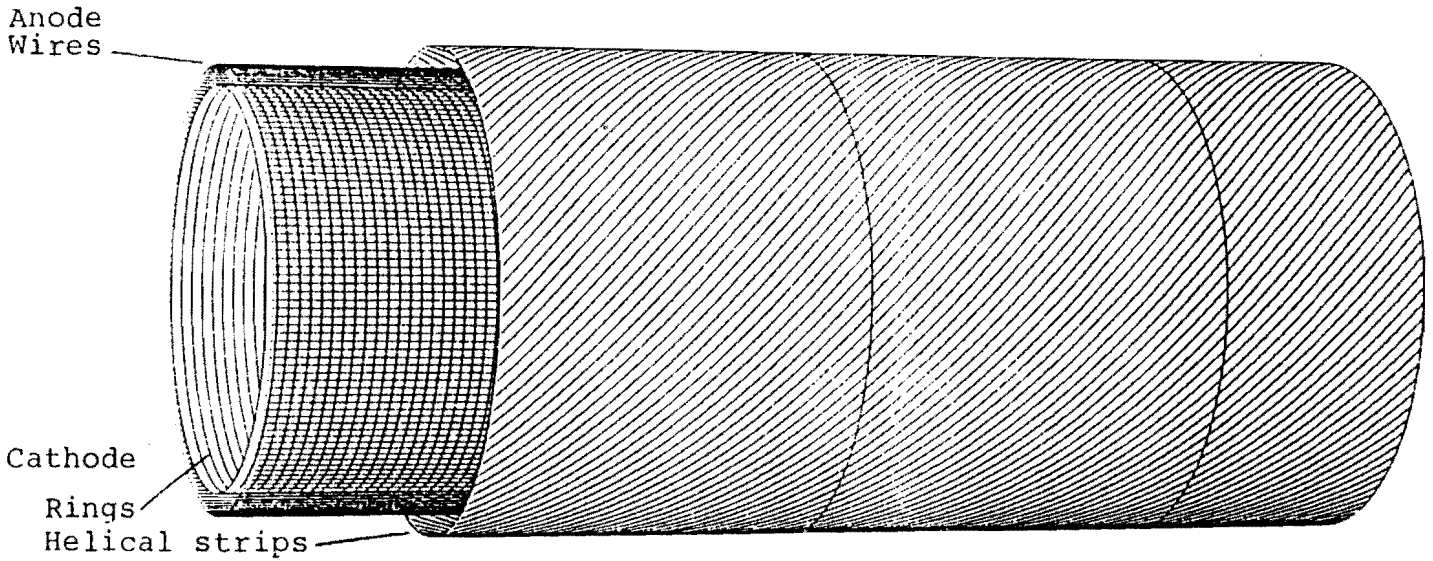

CENTRAL TRACKING CHAMBERS
SENSE ELEMENT ARRANGEMENT

FIGURE 3

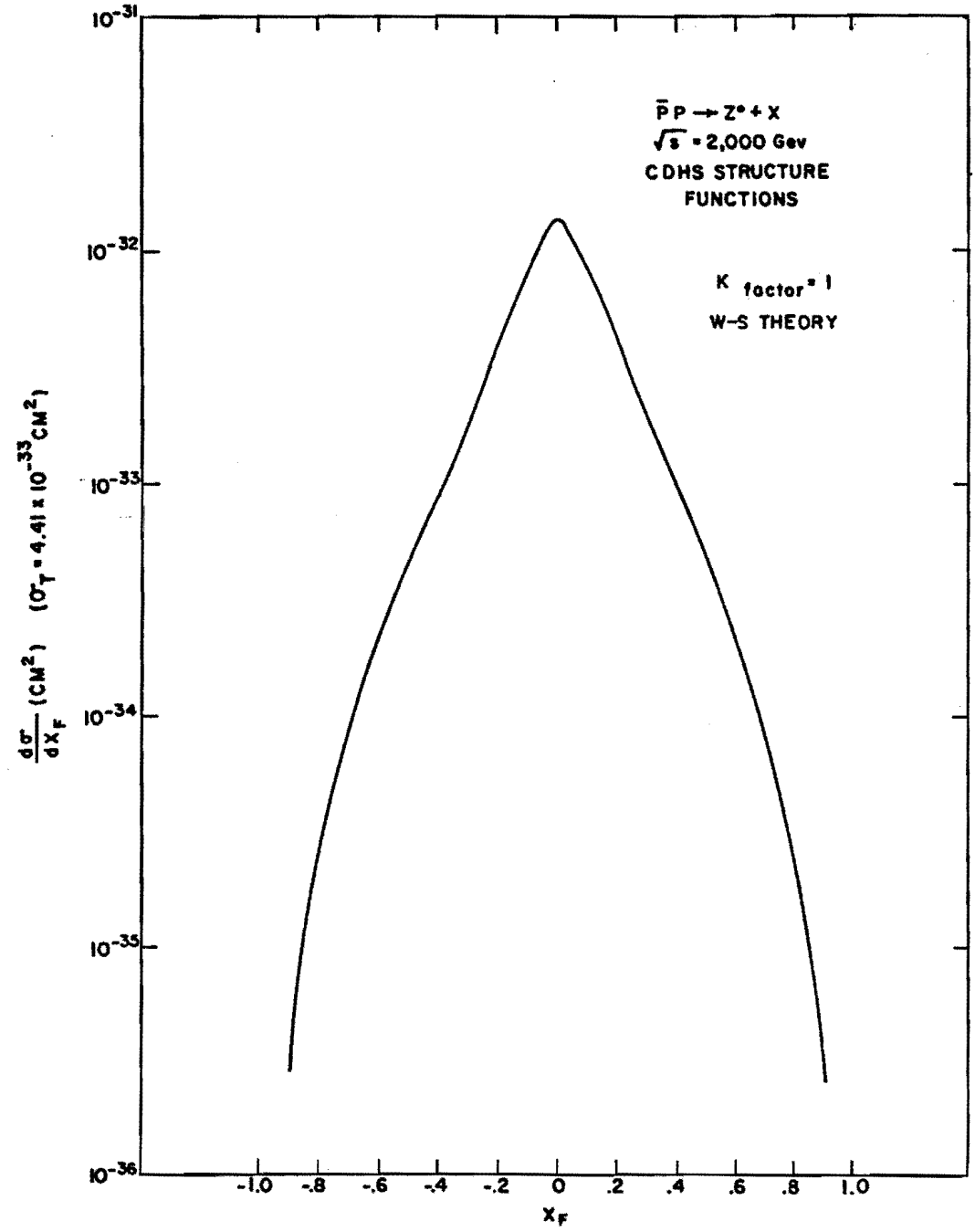
$\bar{P}P \rightarrow Z^0 + X$
$\sqrt{s}$ = 2,000 Gev
CDHS STRUCTURE FUNCTIONS
K factor = 1
W-S THEORY
$\frac{d\sigma}{dX_F}$ (CM^2) (σ_T = 4.41 x 10^{-33} CM^2)
10^{-31}
10^{-32}
10^{-33}
10^{-34}
10^{-35}
10^{-36}
-1.0 -.8 -.6 -.4 -.2 0 .2 .4 .6 .8 1.0
X_F

FIG. 4

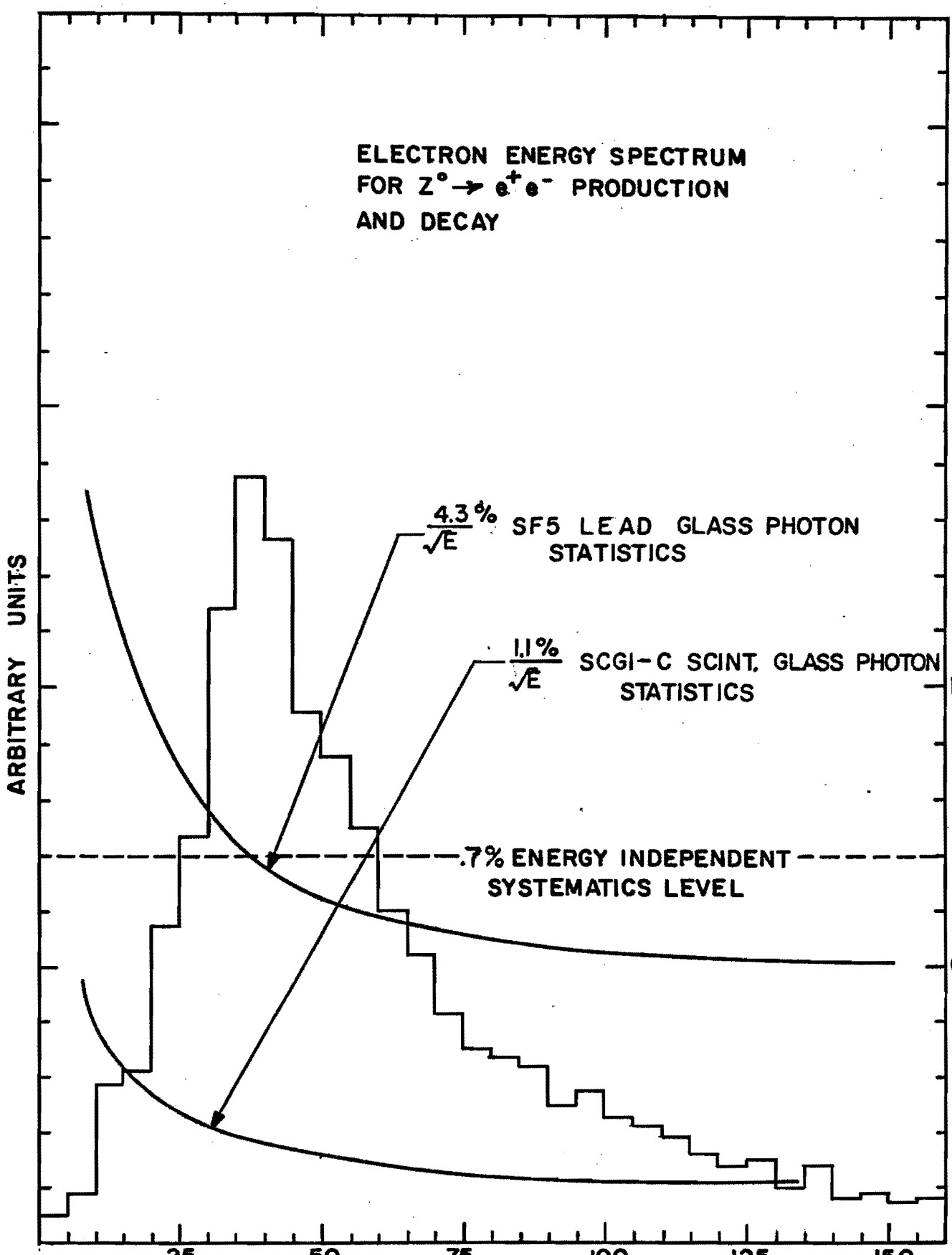
ELECTRON ENERGY SPECTRUM
FOR Z° → e⁺e⁻ PRODUCTION
AND DECAY
4.3%/√E SF5 LEAD GLASS PHOTON STATISTICS
1.1%/√E SCGI-C SCINT. GLASS PHOTON STATISTICS
.7% ENERGY INDEPENDENT SYSTEMATICS LEVEL
ARBITRARY UNITS
CONTRIBUTIONS TO Ee⁻ ENERGY RESOLUTION σ (%)
2.0
1.5
1.0
0.5
25
50
75
100
125
150
Ee⁻ (Gev)

FIG. 5

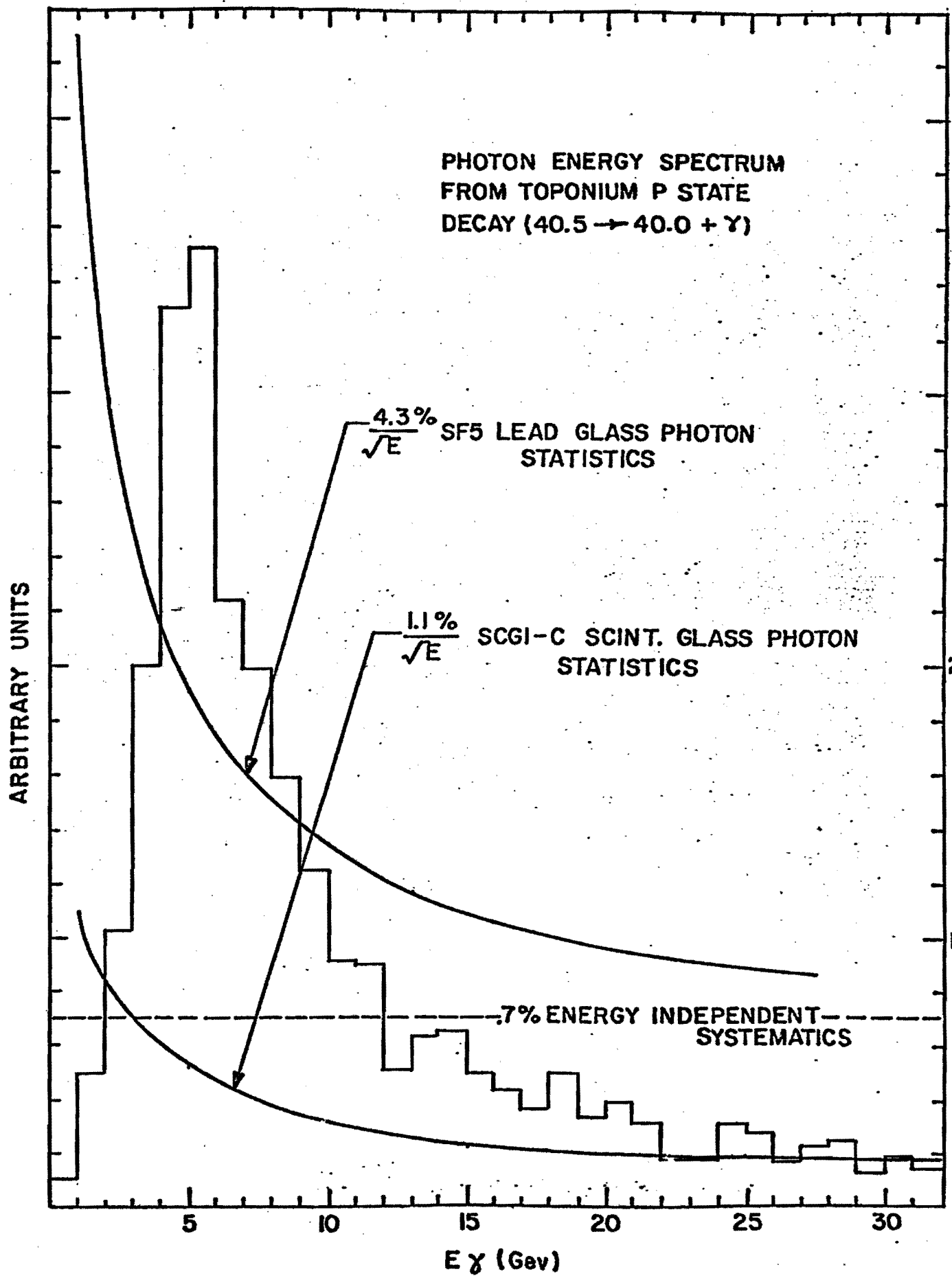
PHOTON ENERGY SPECTRUM
FROM TOPONIUM P STATE
DECAY (40.5 → 40.0 + γ)
4.3%/√E SF5 LEAD GLASS PHOTON STATISTICS
1.1%/√E SCGI-C SCINT. GLASS PHOTON STATISTICS
.7% ENERGY INDEPENDENT SYSTEMATICS
ARBITRARY UNITS
CONTRIBUTIONS TO Eγ ENERGY RESOLUTION σ(%)
Eγ (Gev)
5
10
15
20
25
30
1.
2.
3.
.4

FIG. 6

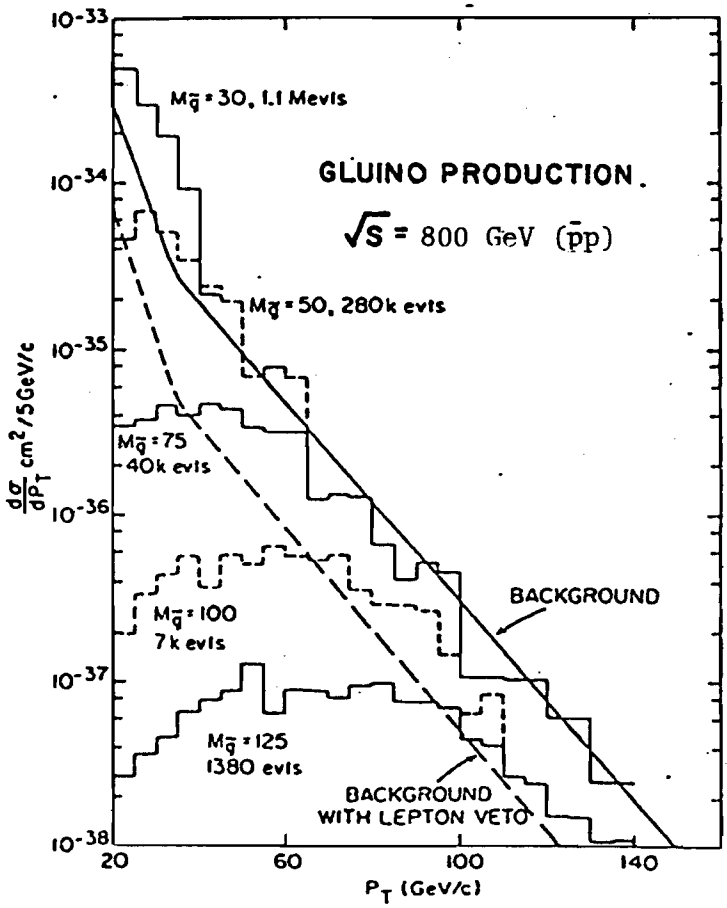
GLUINO PRODUCTION.
$\sqrt{s}$ = 800 GeV ($\bar{p}p$)
$M_{\tilde{g}}$ = 30, 1.1 Mevts
$M_{\tilde{g}}$ = 50, 280k evts
$M_{\tilde{g}}$ = 75
40k evts
$M_{\tilde{g}}$ = 100
7k evts
$M_{\tilde{g}}$ = 125
1380 evts
BACKGROUND
BACKGROUND
WITH LEPTON VETO
$\frac{d\sigma}{dP_T}$ cm²/5GeV/c
10^{-33}
10^{-34}
10^{-35}
10^{-36}
10^{-37}
10^{-38}
20
60
100
140
P_T (GeV/c)

FIG. 7

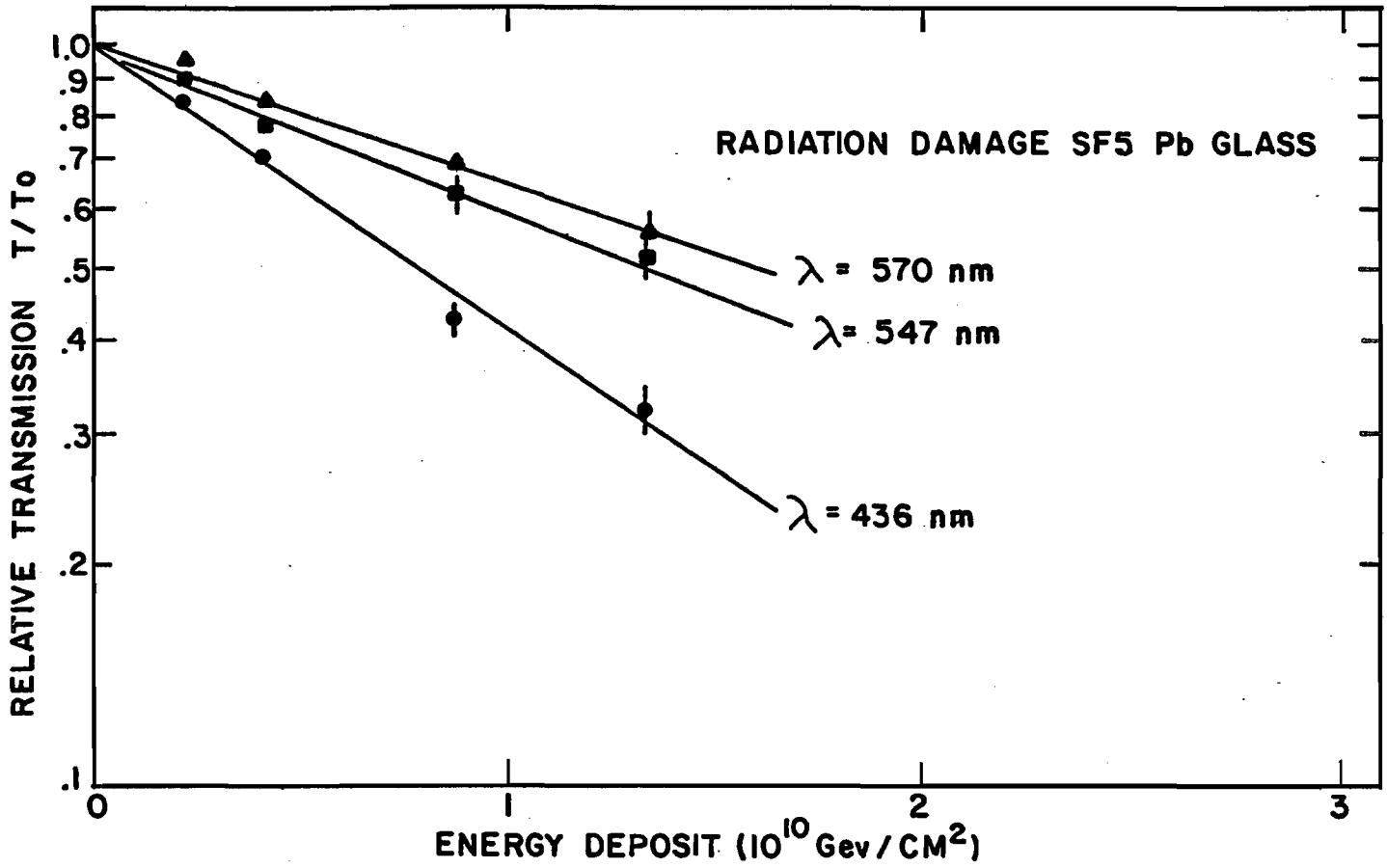
RADIATION DAMAGE SF5 Pb GLASS
λ = 570 nm
λ= 547 nm
λ = 436 nm
RELATIVE TRANSMISSION T/To
1.0
.9
.8
.7
.6
.5
.4
.3
.2
.1
0
1
2
3
ENERGY DEPOSIT (10^10 Gev/CM^2)

FIG. 8a

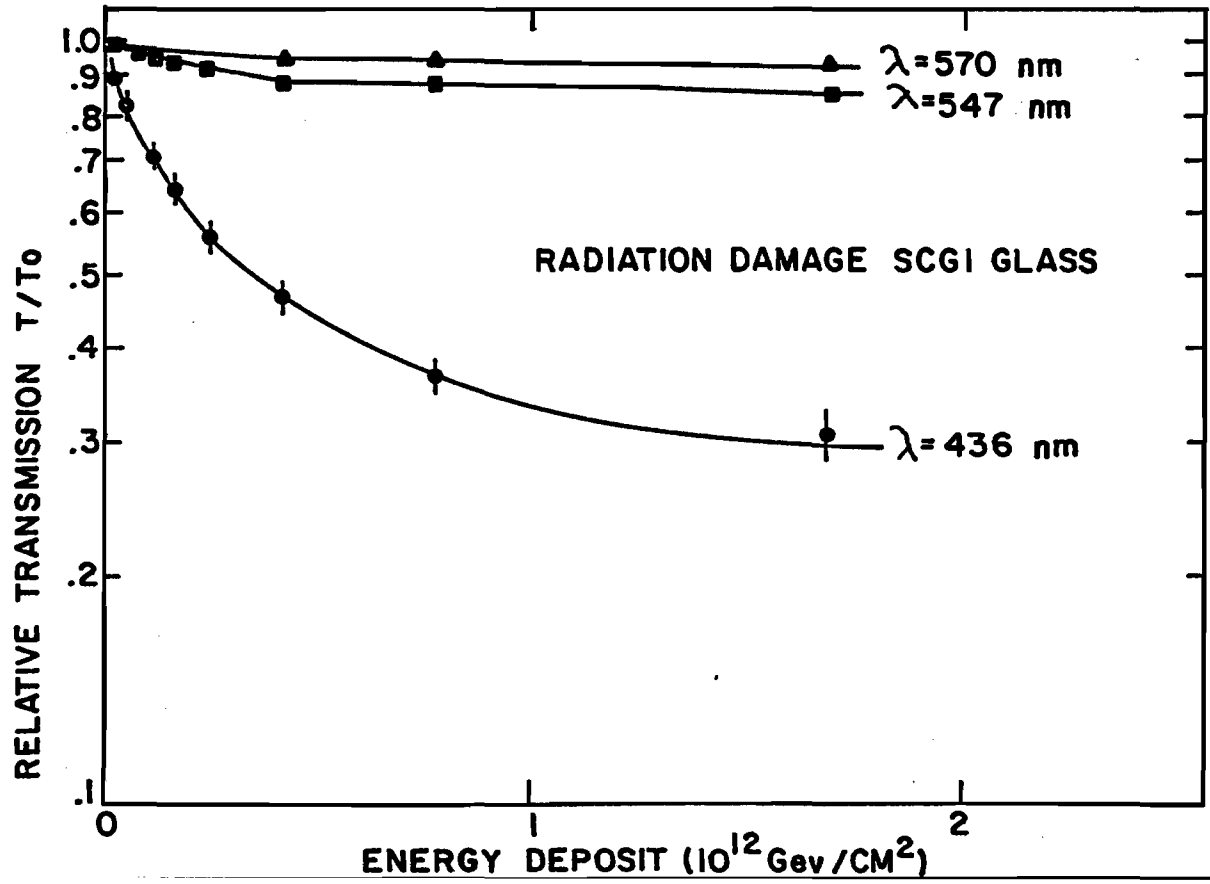
λ=570 nm
λ=547 nm
RADIATION DAMAGE SCGI GLASS
λ=436 nm
RELATIVE TRANSMISSION T/To
1.0
.9
.8
.7
.6
.5
.4
.3
.2
.1
0
1
2
ENERGY DEPOSIT (10^12 Gev/CM^2)